WARWICK
THE UNIVERSITY OF WARWICK

Original citation:
Patrick, Christopher E., Kumar, Santosh, Gotze, Kathrin, Pearce, Matthew J., Singleton, John, Rowlands, George, Balakrishnan, Geetha, Lees, Martin R., Goddard, Paul and Staunton, Julie B. Field-induced canting of magnetic moments in GdCo5 at finite temperature : first-principles calculations and high-field measurements. Journal of Physics: Condensed Matter . doi:10.1088/1361-648X/aad029

Permanent WRAP URL:
http://wrap.warwick.ac.uk/103804

warwick.ac.uk/lib-publications

Field-induced canting of magnetic moments in GdCo$_5$ at finite temperature: first-principles calculations and high-field measurements

Christopher E. Patrick[1], **Santosh Kumar**[1], **Kathrin Götze**[1], **Matthew J. Pearce**[1], **John Singleton**[2], **George Rowlands**[1], **Geetha Balakrishnan**[1], **Martin R. Lees**[1], **Paul A. Goddard**[1], **Julie B. Staunton**[1]

[1]Department of Physics, University of Warwick, Coventry CV4 7AL, UK
[2]National High Magnetic Field Laboratory, Los Alamos National Laboratory, MS-E536, Los Alamos, New Mexico 87545, USA

E-mail: `c.patrick.1@warwick.ac.uk`

Abstract. We present calculations and experimental measurements of the temperature-dependent magnetization of a single crystal of GdCo$_5$ in magnetic fields of order 60 T. At zero temperature the calculations, based on density-functional theory in the disordered-local-moment picture, predict a field-induced transition from an antiferromagnetic to a canted alignment of Gd and Co moments at 46.1 T. At higher temperatures the calculations find this critical field to increase along with the zero-field magnetization. The experimental measurements observe this transition to occur between 44–48 T at 1.4 K. Up to temperatures of at least 100 K, the experiments continue to observe the transition; however, at variance with the calculations, no strong temperature dependence of the critical field is apparent. We assign this difference to the inaccurate description of the zero-field magnetization of the calculations at low temperatures, due to the use of classical statistical mechanics. Correcting for this effect, we recover a consistent description of the high-field magnetization of GdCo$_5$ from theory and experiment.

Of the various families of magnetic intermetallic compounds formed between rare earths and transition metals (RE-TM), the RECo$_5$ series is notable for two reasons. First, the series includes SmCo$_5$, which remains a technologically important permanent magnet thanks to its excellent performance at high temperature [1, 2]. Second, the relatively simple CaCu$_5$ crystal structure of the RECo$_5$ family [3] means that experimental observations can often be explained in terms of a relatively small number of quantities describing fundamental magnetic interactions [4]. Quantifying these fundamental interactions in RECo$_5$ benefits the study of a wider range of RE-TM magnets having more diverse crystal structures [5].

In general, RE-TM magnets owe many of their excellent properties to the localized $4f$ electrons of the lanthanide elements [6]. The $4f$ electrons can lead to large spin and orbital moments on the RE, while electrostatic interactions of these electrons with their environment (the crystal field) can result in a large single-ion magnetocrystalline anisotropy (MCA) [7]. GdCo$_5$ is a rather interesting member of the RECo$_5$ family because, although each Gd atom carries a large spin moment from having seven unpaired $4f$ electrons, the spherically-symmetric charge cloud associated with these electrons causes the orbital moment and crystal field effects to vanish. Therefore the magnetic anisotropy of GdCo$_5$ is dominated by the MCA of the sublattice of Co atoms, with only a small dipolar contribution from the Gd moments. The magnetic response is determined by a competition between this MCA, the exchange interaction between the Gd and Co sublattices, and the interaction of these sublattices with the external field [8].

The RE-Co exchange interaction in RECo$_5$ is antiferromagnetic, such that in the absence of external fields the spin moments of the RE and Co atoms align antiparallel to each other [9]. GdCo$_5$ is therefore a ferrimagnet, whose resultant moment points in the direction of the Co sublattice moments with a magnitude per formula unit (FU) of approximately $(5 \times 1.8 - 7.3 = 1.7)\mu_\mathrm{B}$ [10]. The exchange field felt by the Gd moments ($\sim$235 T [11]) is very large compared to external fields achievable in the laboratory. Nonetheless, modest fields of just a few T can break the antiparallel alignment of Gd and Co moments, provided that the sample is aligned with its magnetic easy axis (the crystallographic c direction) pointing normal to the applied field [12]. If instead the external field is applied along the easy axis, the antiparallel alignment is expected to be stable up to at least 70 T [13].

An intermediate case has the GdCo$_5$ sample free to rotate in the applied field, which is the natural geometry for powder samples [14]. Radwański et al. [13] predicted that canting between the Gd and Co moments would be induced in this setup with an applied field of 40 T, resulting in an abrupt change of gradient in the magnetization vs field curve. Subsequent measurements in pulsed fields of 60 T reported by Kuz'min et al. [15] confirmed the existence of this feature, which occurred at 46 T at 5 K. More recent work by Isnard et al. [16] on another Gd-Co compound, GdCo$_{12}$B$_6$, was able to demonstrate both the transition from the antiparallel to the canted state, and also the corresponding feature at much higher field marking the transition to parallel (ferromagnetic) Gd-Co alignment. The same work reported magnetization curves at different temperatures

up to 121 K, allowing the temperature dependence of the exchange coupling to be investigated [16].

Although models of ferrimagnets in external fields have been developed at least as far back as 1968 [17], these models generally require experimental parameterization. However, some of us [18] recently introduced a method of calculating temperature-dependent magnetization versus field curves from first principles (FPMVB). We developed the method, which is based on relativistic density-functional theory in the disordered-local-moment picture (DFT-DLM) [19, 20], in order to understand magnetization measurements on GdCo$_5$ orientated with its easy axis normal to a relatively small ($\leq$7 T) applied field. The purpose of this Letter is to show how the same FPMVB approach can be applied to a free-to-rotate sample in much higher ($\leq$ 60 T) fields. We pair our calculations with pulsed-field measurements of a single crystal of GdCo$_5$ in temperatures up to 100 K. These new measurements allow us to compare the theoretical and experimental values of the temperature-dependent critical fields required to induce the transition from the antiparallel to the canted Gd-Co sublattices in GdCo$_5$.

We first discuss our calculations of the magnetization versus field curves. In our previous work [18] we showed how these curves could be calculated either by carefully analyzing the torque on each magnetic moment, or by parametrizing a model expression for the free energy which could then be minimized for a given external field. Here we take the second approach, using the model that we previously found to give an accurate description of the free energy landscape [18]:

$$
\begin{aligned}
F_2(\theta_{\mathrm{Gd}}, \theta_{\mathrm{Co}}) = & -A\,\cos(\theta_{\mathrm{Gd}} - \theta_{\mathrm{Co}}) + K_{1,\mathrm{Co}}\,\sin^2\theta_{\mathrm{Co}} \\
& + K_{2,\mathrm{Co}}\,\sin^4\theta_{\mathrm{Co}} + K_{1,\mathrm{Gd}}\,\sin^2\theta_{\mathrm{Gd}} \\
& + S(\theta_{\mathrm{Gd}}, \theta_{\mathrm{Co}}).
\end{aligned}
\tag{1}
$$

The angles θ_{Gd} and θ_{Co} are given with respect to the crystallographic c axis, as shown in the inset of Figure 1(a). The quantities A, $K_{i,\mathrm{X}}$ and S are all dependent on temperature. A describes the antiferromagnetic Gd-Co exchange, while the various $K_{i,\mathrm{X}}$ values quantify the MCA of the individual sublattices originating from the spin-orbit interaction. Note that although the Gd-4f electrons do not contribute to the MCA, the Gd-5d moments induced by the 4f-5d and 3d-5d exchange interactions [21] do result in a small positive value for $K_{1,\mathrm{Gd}}$. $K_{1,\mathrm{Co}}$ consists of contributions both from the 2c and 3g crystal sites, as discussed in the literature for the isostructural YCo$_5$ compound [22, 23]. $S(\theta_{\mathrm{Gd}}, \theta_{\mathrm{Co}})$ is the contribution to the MCA from dipole-dipole interactions, and has the explicit form [24]:

$$
\begin{aligned}
S(\theta_{\mathrm{Gd}}, \theta_{\mathrm{Co}}) = & S_1\,\sin^2\theta_{\mathrm{Gd}} + S_2\,\sin^2\theta_{\mathrm{Co}} + S_3 \times \\
& \left(\sin\theta_{\mathrm{Gd}}\sin\theta_{\mathrm{Co}} - \frac{2}{3}\cos(\theta_{\mathrm{Gd}} - \theta_{\mathrm{Co}}) \right).
\end{aligned}
$$

The additional contribution to the free energy due to an external field $\vec{B}$ is $-\sum_i \vec{B} \cdot \vec{M_i}$, where $\vec{M_{\mathrm{Gd}}}$ and $\vec{M_{\mathrm{Co}}}$ are the magnetizations of the two sublattices. While M_{Gd} is independent of magnetization direction, the calculations showed a temperature-dependent magnetization anisotropy on the Co sublattice [18], well described by the

expression $M_{\mathrm{Co}}(\theta_{\mathrm{Co}}) = M_{\mathrm{Co}}^0[1 - p\sin^2\theta_{\mathrm{Co}}]$. For a field applied at an angle γ to the c axis, our expression for the free energy is therefore

$$
\begin{aligned}
F_2^{\mathrm{Tot}}(\theta_{\mathrm{Gd}}, \theta_{\mathrm{Co}}, \gamma, B) = {} & F_2(\theta_{\mathrm{Gd}}, \theta_{\mathrm{Co}}) \\
& + BM_{\mathrm{Gd}}\cos(\theta_{\mathrm{Gd}} - \gamma) \\
& - BM_{\mathrm{Co}}^0\cos(\theta_{\mathrm{Co}} - \gamma) \times \\
& [1 - p\sin^2\theta_{\mathrm{Co}}].
\end{aligned}
\tag{2}
$$

Assuming that the GdCo₅ sample is able to reach its equilibrium state, the magnetization measured along the field direction $\sum_i \vec{B} \cdot \vec{M}_i$ is determined by the set of angles $\{\theta_{\mathrm{Gd}}, \theta_{\mathrm{Co}}, \gamma\}$ which minimize F_2^{Tot}. In the case that the sample is clamped, γ is fixed according to the experimental geometry.

We emphasize that the sublattice magnetizations M_{Co} and M_{Gd} depend on the temperature T. In the disordered-local-moment picture of magnetism, $\vec{M}_{\mathrm{X}} = \mu_{\mathrm{X}}\vec{m}_{\mathrm{X}}(T)$, where μ_{X} is the local moment magnitude (e.g. $\sim 7\mu_{\mathrm{B}}$ for Gd) and $\vec{m}_{\mathrm{X}}$ is an order parameter quantifying the configurationally-averaged orientation of the local moment. The magnitude of $\vec{m}_{\mathrm{X}}$ varies from one at 0 K to zero at the Curie temperature T_{C}. We note that, in principle, $\vec{m}_{\mathrm{X}}$ should also depend on external field, e.g. to describe paramagnetic behaviour. However, given the high T_{C} of GdCo₅ (~ 1000 K), up to room temperature we expect the external field to have a minor effect on the order parameter compared to thermal fluctuations. Therefore, in our calculations we always use the zero-field values of m_{X}.

We performed the numerical minimization of F_2^{Tot} using the standard Broyden-Fletcher-Goldfarb-Shanno scheme as implemented in the `SciPy` distribution [25]. The temperature-dependent quantities A, $K_{i,\mathrm{X}}$ etc. required to construct F_2^{Tot} were calculated from first principles in our previous paper [18] and are reproduced in the Supplementary Material.

In Figure 1(a) we show the magnetization versus field curve calculated by minimizing F_2^{Tot} at $T = 0$ K. As in experiment, the magnetization is measured along the field direction. Up to 46.1 T the applied field does not induce any change in the magnetization, which remains at the value $M_{\mathrm{Co}}^0 - M_{\mathrm{Gd}} = 1.60\mu_{\mathrm{B}}/\mathrm{FU}$. At this critical value B_{C}, there is a kink in the magnetization curve. Above B_{C} the measured magnetization becomes effectively linear with respect to the applied field, and at much higher fields (463 T, not shown) the magnetization saturates to $M_{\mathrm{Co}}^0 + M_{\mathrm{Gd}}$.

Further insight into the behaviour of the magnetization can be obtained by plotting the field dependence of the magnetization angles θ_{Gd} and θ_{Co}, and of the angle γ between the easy c axis and the applied field [Figure 1(b)]. At B_{C} the sample undergoes a sudden rotation (increase in γ) accompanied by a rotation of the sublattice magnetizations away from the easy axis. The Co sublattice rotates by a relatively small amount compared to the Gd sublattice (1.7° compared to 7.3° at 60 T, respectively). As indicated by the schematics in Figure 1(b), the effect of these rotations is to reduce the misalignment of the Gd magnetization with the external field. This reduction in misalignment is, therefore, the physical driver of the transition to the canted state. Precisely how this
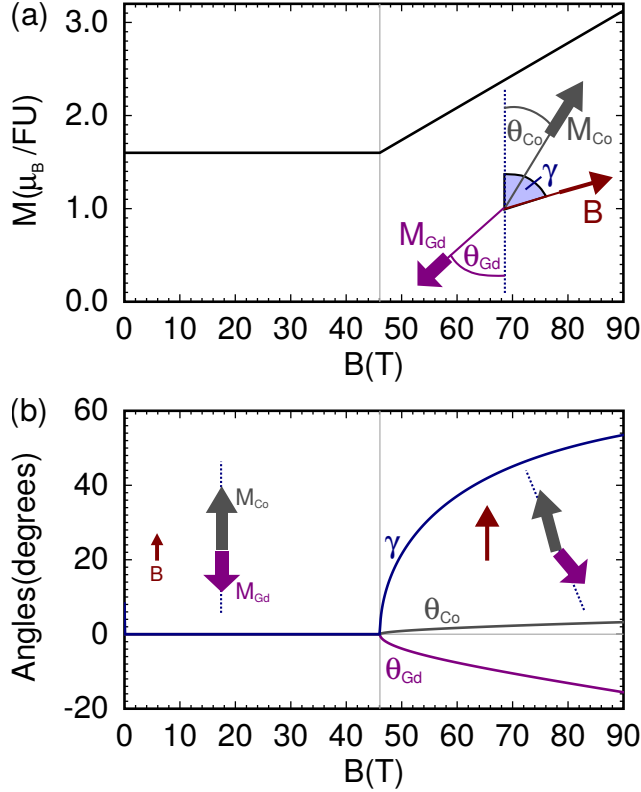
Figure 1. (a) Magnetization vs field curve calculated at $T = 0$ K for a GdCo$_5$ sample free to rotate in the applied field. The inset illustrates the angles used in the definition of F_2^{Tot}, with the dotted line representing the crystallographic c axis. The vertical grey line marks the transition from antiparallel to canted magnetic sublattices. (b) Calculated variation of the angles $\{\theta_{\text{Gd}}, \theta_{\text{Co}}, \gamma\}$ at $T = 0$ K. The arrows illustrate the orientations of the magnetic sublattices with respect to the applied field.

misalignment is reduced is a balance of the energy penalties associated with breaking the antiparallel alignment of the Co and Gd sublattices, of misaligning the Co magnetization with the external field, and of rotating the individual sublattice magnetizations away from the easy axis. As we show below, this latter anisotropy penalty is weak compared to the exchange and external contributions.

If the sample is not allowed to rotate freely, but rather clamped with its easy axis parallel to the field direction ($\gamma = 0°$), the field required to induce the transition to a canted magnetic state is calculated to be 92.4 T. However, if the sample is held perpendicular to the field ($\gamma = 90°$) the moments adopt a canted arrangement for an arbitrarily small field, as observed experimentally [12, 18].

In Figure 2(a) we show the magnetization curves calculated using F_2^{Tot} and the temperature-dependent parameters, up to 300 K. The increasing zero-field magnetization as a function of temperature is a consequence of the ferrimagnetic nature of GdCo$_5$, where the Gd moments disorder more quickly with temperature than Co [10]. Accordingly, the resultant $M_{\text{Co}}^0 - M_{\text{Gd}}$ initially increases with temperature, although as we discuss later the calculated rate of increase exceeds what is observed experimentally.
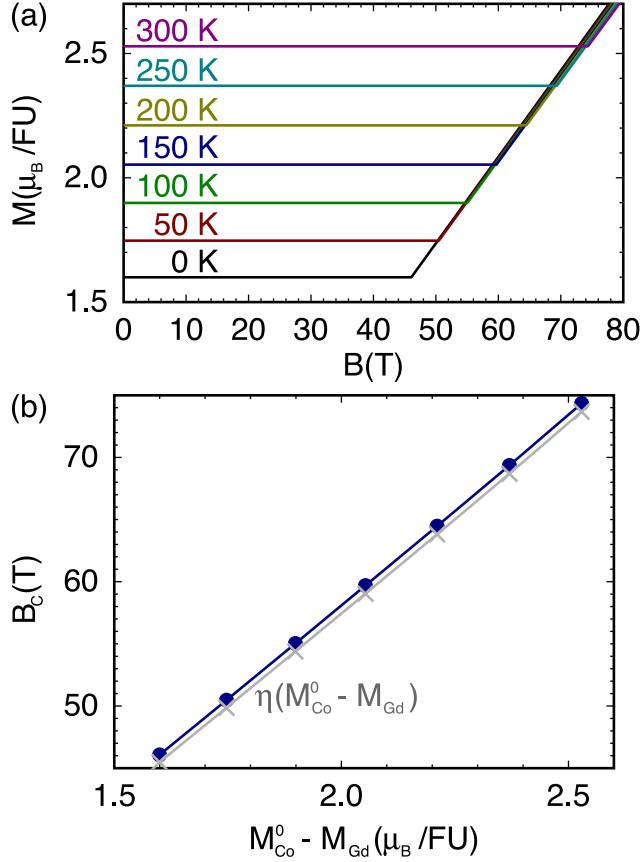
Figure 2. (a) Magnetization vs field curves calculated using F_2^{Tot} and temperature-dependent parameters. (b) Critical magnetic fields B_{C} at which the magnetization displays a kink, extracted from the curves of (a) (blue circles) or calculated using the expression $\eta(M_{\mathrm{Co}}^0 - M_{\mathrm{Gd}})$ (grey crosses), where $\eta \equiv A/(M_{\mathrm{Co}}^0 M_{\mathrm{Gd}})$ (see text). The lines joining the symbols are guides to the eye.

All of the curves have the same qualitative form as the $T = 0$ K case, and the magnetizations for $B > B_{\mathrm{C}}$ lie almost on top of each other.

Like the zero-field magnetization, B_{C} increases monotonically with temperature. In Figure 2(b) we plot B_{C} as a function of $M_{\mathrm{Co}}^0 - M_{\mathrm{Gd}}$ to show that there is effectively a linear relation between the two quantities. To understand this behaviour further it is useful to consider a simpler two-sublattice model [4], where the free energy is modelled as

$$
\begin{aligned}
F_3^{\mathrm{tot}} = {} & -A\,\cos(\theta_{\mathrm{Gd}} - \theta_{\mathrm{Co}}) + K_{1,\mathrm{Co}}\,\sin^2\theta_{\mathrm{Co}} \\
& + B[M_{\mathrm{Gd}}\cos(\theta_{\mathrm{Gd}} - \gamma) - M_{\mathrm{Co}}^0\cos(\theta_{\mathrm{Co}} - \gamma)].
\end{aligned}
\tag{3}
$$

Minimizing this model expression analytically yields three simple results: first, that for $K_{1,\mathrm{Co}} \geq 0$ the Co moments always lie along the easy axis, i.e. $\theta_{\mathrm{Co}} = 0$ or $180°$; second, that $B_{\mathrm{C}} = \eta[M_{\mathrm{Co}}^0 - M_{\mathrm{Gd}}]$ where $\eta \equiv A/(M_{\mathrm{Gd}}M_{\mathrm{Co}}^0)$; and third, that the measured magnetization above B_{C} is given by $M(B) = B/\eta$, until the upper critical field of $\eta[M_{\mathrm{Co}}^0 + M_{\mathrm{Gd}}]$ is reached.

We recalculated the magnetization vs field curves using F_3^{tot} and obtained results

that, on the scale of Figure 2(a), are indistinguishable from those obtained from F_2^{tot}. In Figure 2(b) we plot B_C predicted from F_3^{tot} as grey crosses. The two sets of B_C closely resemble each other, with the plot scale obscuring the variation in the offset of 0.59–0.67 T. Part of this offset is due to the dipolar anisotropy S_3 renormalizing A, and the rest due to the anisotropy energy of the Gd sublattice.

As indicated by the near-linearity of the crosses in Fig. 2(b), our calculated values of η depend only weakly on temperature, varying from 28.4–29.5 T/(μ_B/FU) over the 0–300 K range. This small variation is consistent with the high-field study on the related material GdCo$_{12}$B$_6$ [16], which could not resolve any temperature variation of η between 4.2 and 63 K.

Our calculated value of 46.1 T for B_C at zero temperature agrees rather well with the value of 46 T measured at 5 K by Kuz'min et al. [15]. However, to our knowledge measurements on GdCo$_5$ at higher temperatures have not been reported in the literature. Therefore, using the single crystal of GdCo$_5$ grown by some of us recently using the floating zone technique [10], we carried out high-field measurements at temperatures between 1.4 and 100 K. The pulsed-field magnetization measurements were performed at the National High Magnetic Field Laboratory in Los Alamos; fields of up to 60 T with typical rise times $\approx$ 10 ms were used. The single crystal, free to rotate, is placed in a 1.3 mm diameter polychlorotrifluoroethylene ampoule (inner diameter 1.0 mm) that can be moved into and out of a 1500-turn, 1.5 mm bore, 1.5 mm long compensated-coil susceptometer, constructed from 50 gauge high-purity copper wire [26]. When the sample is within the coil and the field pulsed the voltage induced in the coil is proportional to the rate of change of magnetization with time. Accurate values of the magnetization are obtained by numerical integration of the signal with respect to time, followed by subtraction of the integrated signal recorded using an empty coil under the same conditions. The magnetic field is measured via the signal induced within a coaxial 10-turn coil and calibrated via observation of de Haas-van Alphen oscillations arising from the copper coils of the susceptometer.

Figure 3 shows the experimental magnetization vs field curves measured in a pulsed field of 60 T, at 1.4 K and 100 K. The experimental curves show more features than the idealized calculations. In particular, since the sample is initially demagnetized and randomly oriented as the field is switched on, it undergoes a variable amount of motion which results in large fluctuations in the low-field magnetization. Similarly as the field is reduced to zero the sample demagnetizes, which is not accounted for in the calculations. In general the experiments do not show a region of strictly constant magnetization unlike the calculations, which neglect the field dependence of the order parameter as discussed above. However, the experimental curves do exhibit the same critical behaviour at high fields, namely a kink in the magnetization curve. At 1.4 K this kink occurs at 44 T, reasonably close to the previously reported value of 46 T at 5 K [15].

In order to perform a quantitative comparison between calculations and experiment up to 100 K, we developed a protocol to extract B_C from the experimental data in a consistent way. The protocol consists of first separating each set of data into two
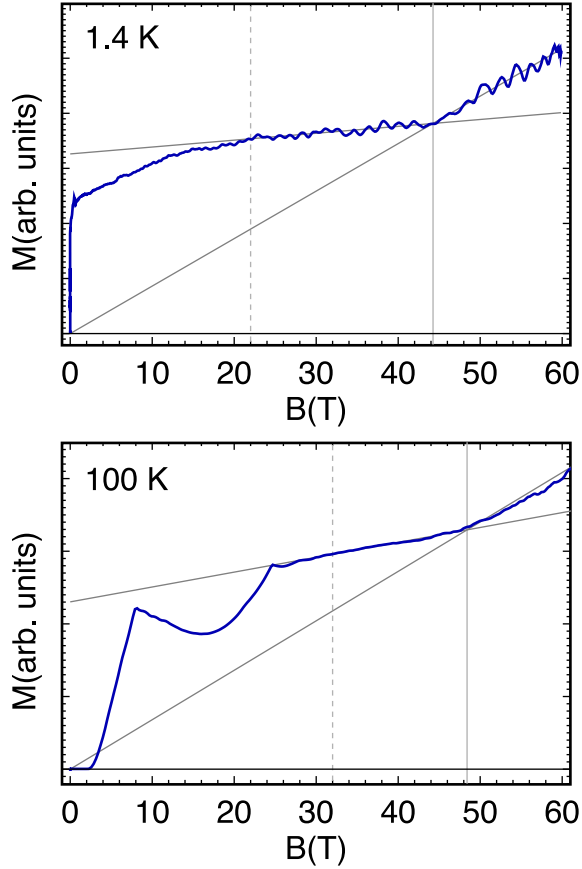
Figure 3. Experimentally-measured magnetization vs field curves at 1.4 and 100 K (blue). The horizontal black line is the zero axis; the y-axis scale is arbitrary. The grey lines are explained in the text.

curves, corresponding to an increasing and decreasing magnetic field, and analyzing them separately. For instance, in Figure 3 the 1.4 K and 100 K data were taken for decreasing and increasing field, respectively. Next we discard the data at low fields where the signal is dominated by the sample motion and (de)magnetization. The rejected data falls to the left of the dashed vertical lines in Figure 3. We then partition the remaining data into two regions and fit the data within each region with a straight line. The partitioning is performed under the constraints that (a) the two fitted lines join at the partition and (b) the second line intersects the origin. Constraint (b) is guided by the numerical results of Figures 1 and 2 which showed the high-field magnetization to effectively satisfy this constraint (the relation is exact for F_3^{Tot}). The straight lines fits are shown in grey in Figure 3. The field at which the two lines join (i.e. the partition) is taken as the experimental B_{C}, indicated by the solid vertical line.

We applied the described protocol to all of the magnetization curves measured at different temperatures. In all but two cases the procedure gave unambiguous values for B_{C}, which we plot in Figure 4. All of the measured curves, including the two failed cases, are shown in the Supplementary Material.

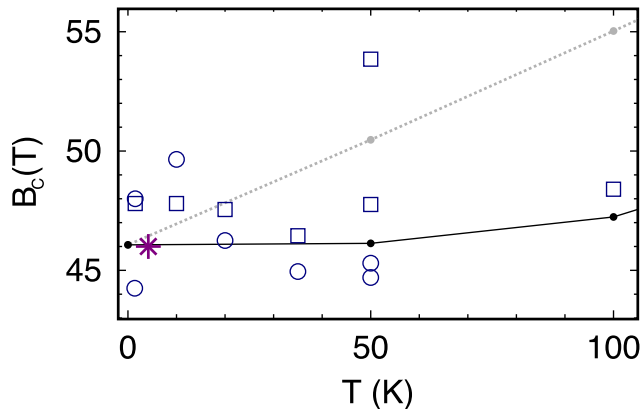Apart from an anomalous value of 54 T at 50 K, the experimental values of B_{C}

Figure 4. Critical magnetic fields B_C extracted from our magnetization curves, either for increasing (squares) or decreasing (open circles) applied field. The star is the previously reported value of 46 T [15]. The filled circles joined by straight lines are the calculated values of B_C, with the grey values corresponding to Figure 2(b) and the black values corrected for the experimental magnetization, as discussed in the text.

lie in the 44–50 T region. For the same pulse there is a difference of 1–2 T depending on whether the increasing or decreasing applied field is analyzed (squares or circles in Figure 4). However, at variance with the calculated values of B_C (grey circles and dotted lines) the experiments do not show any particular increase in critical field with temperature.

To resolve this apparent discrepancy we return to Figure 2(b), which shows how B_C is essentially linear in the zero-field magnetization $M^0 = M_{Co}^0 - M_{Gd}$. Unfortunately, the DFT-DLM theory used to calculate the parameters determining the free energy does not describe the temperature dependence of the magnetization very well at low temperatures. This is because the DFT-DLM statistical mechanics is based on a classical Heisenberg ($J = \infty$) description of spins [19], with no barrier to rotating the spins at zero temperature. So, while the calculations predict the GdCo₅ zero-field magnetization to increase by $0.3\mu_B$/FU between 0–100 K, experimentally the increase is in fact just $0.04\mu_B$/FU [10].

To correct for this effect, we rescale the DFT-DLM critical fields as $B_C^{corr}(T) = B_C(0) + \Delta B_C(T) \times \Delta M_{exp}^0(T)/\Delta M_{calc}^0(T)$, where ΔM^0 denotes the change in zero-field magnetization with temperature, either measured experimentally or calculated. $B_C(T)$ are the uncorrected critical fields, with $\Delta B_C(T) = B_C(T) - B_C(0)$. Plotting the rescaled fields as the black circles in Figure 4 we see how, even with the temperature dependence of η included, the calculated change in B_C^{corr} over the 0–100 K temperature range is now only of the order of 1 T, which is below the resolution of the experiment. Therefore our interpretation is that the lack of variation in B_C observed experimentally is consistent with the theory, once the low temperature behaviour of the DFT-DLM calculations has been accounted for. The experimental observations are also consistent with the previously-reported measurements on GdCo₁₂B₆ [16] which found a similarly small variation in critical field with temperature.

In summary, we have demonstrated how the FPMVB method, developed and parametrized to calculate magnetization curves at low applied fields, can also be used to calculate high-field behaviour. Close to zero temperature, there is good agreement between the predictions of the theory and experiment. At higher temperatures, the qualitative predictions of the model remain accurate to at least 100 K, where we continued to observe the predicted kink in the magnetization curve; however, to obtain quantitative agreement in the temperature dependence of the critical magnetic field it is necessary to correct for the classical statistical mechanics employed in the calculations. Interesting avenues for future exploration include more complicated magnetic systems consisting of multiple magnetic sublattices, as well as systems where competing anisotropies lead to unusual magnetization behaviour, e.g. first-order magnetization processes [27].

Acknowledgments

References

[1] Strnat K, Hoffer G, Olson J, Ostertag W and Becker J J 1967 *J. Appl. Phys.* **38** 1001
[2] Gutfleisch O, Willard M A, Brück E, Chen C H, Sankar S G and Liu J P 2011 *Adv. Mater.* **23** 821
[3] Kumar K 1988 *J. Appl. Phys.* **63** R13
[4] Radwański R 1986 *Physica B+C* **142** 57
[5] Franse J J M and Radwański R J 1993 *Handbook of Magnetic Materials* vol 7 (Elsevier North-Holland, New York) chap 5, p 307
[6] Elliott R J 1972 *Magnetic Properties of Rare Earth Metals* ed Elliott R J (London and New York: Plenum Press) p 1
[7] Kuz'min M D and Tishin A M 2008 *Handbook of Magnetic Materials* vol 17 (Elsevier B.V.) chap 3, p 149
[8] Yermolenko A S 1980 *Fiz. Metal. Metalloved.* **50** 741
[9] Nesbitt E A, Williams H J, Wernick J H and Sherwood R C 1962 *J. Appl. Phys.* **33** 1674
[10] Patrick C E, Kumar S, Balakrishnan G, Edwards R S, Lees M R, Mendive-Tapia E, Petit L and Staunton J B 2017 *Phys. Rev. Materials* **1** 024411
[11] Loewenhaupt M, Tils P, Buschow K and Eccleston R 1994 *J. Magn. Magn. Mater.* **138** 52
[12] Ballou R, Déportes J, Gorges B, Lemaire R and Ousset J 1986 *J. Magn. Magn. Mater.* **54–57** 465
[13] Radwański R, Franse J, Quang P and Kayzel F 1992 *J. Magn. Magn. Mater.* **104** 1321
[14] Liu J, de Boer F, de Châtel P, Coehoorn R and Buschow K 1994 *J. Magn. Magn. Mater.* **132** 159

[15] Kuz'min M D, Skourski Y, Eckert D, Richter M, Müller K H, Skokov K P and Tereshina I S 2004 *Phys. Rev. B* **70** 172412

[16] Isnard O, Skourski Y, Diop L V B, Arnold Z, Andreev A V, Wosnitza J, Iwasa A, Kondo A, Matsuo A and Kindo K 2012 *J. Appl. Phys.* **111** 093916

[17] Clark A E and Callen E 1968 *J. Appl. Phys.* **39** 5972

[18] Patrick C E, Kumar S, Balakrishnan G, Edwards R S, Lees M R, Petit L and Staunton J B 2018 *Phys. Rev. Lett.* **120** 097202

[19] Györffy B L, Pindor A J, Staunton J, Stocks G M and Winter H 1985 *J. Phys. F: Met. Phys.* **15** 1337

[20] Staunton J B, Szunyogh L, Buruzs A, Györffy B L, Ostanin S and Udvardi L 2006 *Phys. Rev. B* **74** 144411

[21] Burzo E, Chioncel L, Tetean R and Isnard O 2011 *J. Phys.: Condens. Matter* **23** 026001

[22] Thuy N, Franse J, Hong N and Hien T 1988 *J. Phys. Colloq.* **49** C8–499–C8–504

[23] Steinbeck L, Richter M and Eschrig H 2001 *Phys. Rev. B* **63** 184431

[24] Ballou R, Déportes J and Lemaire J 1987 *J. Magn. Magn. Mater.* **70** 306

[25] Jones E, Oliphant T, Peterson P *et al.* 2001– SciPy: Open source scientific tools for Python URL `http://www.scipy.org/`

[26] Goddard P A, Singleton J, Sengupta P, McDonald R D, Lancaster T, Blundell S J, Pratt F L, Cox S, Harrison N, Manson J L, Southerland H I and Schlueter J A 2008 *New J. Phys.* **10** 083025

[27] Thang C, Brommer P, Colpa J, Thuy N and Franse J 1996 *Physica B: Condensed Matter* **228** 205